Journal of Systems Engineering and Electronics
Vol. 34, No. 5, October 2023, pp.1158 – 1170

Super-resolution parameter estimation of monopulse radar by wide-narrowband joint processing

CAI Tianyi[1], DAN Bo[2,*], and HUANG Weibo[1]

1. Sichuan Institute of Aerospace Electronic Equipment, Chengdu 610100, China;
2. Coastal Defense College, Naval Aviation University , Yantai 264001, China

Abstract: The angular resolution of radar is of crucial significance to its tracking performance. In this paper, a super-resolution parameter estimation algorithm based on wide-narrowband joint processing is proposed to improve the angular resolution of wideband monopulse radar. The range cells containing resolvable scattering points are detected in the wideband mode, and these range cells are adopted to estimate part of the target parameters by algorithms of low computational requirement. Then, the likelihood function of the echo is constructed in the narrow-band mode to estimate the rest of the parameters, and the parameters estimated in the wideband mode are employed to reduce computation and enhance estimation accuracy. Simulation results demonstrate that the proposed algorithm has higher estimation accuracy and lower computational complexity than the current algorithm and can avoid the risk of model mismatch.

Keywords: monopulse radar, super-resolution, wide-narrow band processing, parameter estimation.

DOI: 10.23919/JSEE.2023.000132

1. Introduction

Multiple targets in combination that cannot be resolved by radar are called the unresolved targets. The existence detection of unresolved targets and the super-resolution estimation of angle and range parameters of unresolved targets have always been the focus of academic research [1].

Regarding the existence detection of unresolved targets, a generalized likelihood ratio test (GLRT) algorithm was proposed based on the monopulse ratio [2]. Further, the GLRT idea is extended to the case that three targets are unresolvable [3]. A detection algorithm was designed with the real part of monopulse ratio [4]. An algorithm based on maximum likelihood estimation (MLE) is presented [5], which outperforms the GLRT algorithm but requires much more computation. Later, a model-free algorithm is established [6]. This algorithm outperforms the GLRT algorithm and needs much less computation than the algorithm in [5].

Concerning super-resolution parameter estimation of unresolved targets, it is suggested that the target is located between the adjacent sampling points in the range dimension. The adjacent sampling points are adopted to estimate unresolved point target parameters by MLE, which is referred to as the point target estimation (PTE) algorithm [7]. With the same idea, a super-resolution estimation algorithm for unresolved extended targets named as monopulse radar signal processing with an extended target model (MRSP-E) is proposed [8]. The model in [7] was extended to the case where the signal envelope after pulse compression is a sinc function [9]. Additionally, an algorithm based on reversible jump Markov chain Monte Carlo (RJ-MCMC) [10] is built to achieve a similar estimation accuracy as in [7], while it requires fewer subpulses. Because not all targets are completely unresolvable, some of the sampling points may sample the echoes from the resolvable parts of the targets. With this advantage, the signal to noise ratio (SNR) of the targets is estimated by the sampling points of resolvable parts [11]. However, this neglects the identification of those sampling points. Estimation algorithms based on array antennas are presented [12−17] but are not applicable to non-array radars. Moreover, algorithms requiring the radar antenna to be in the scanning state are established [18−21]. This is only applicable to the search stage of radars and has a limited scope of application. In [22,23], a super-resolution imaging method was proposed, but required electromagnetic orbital angular momentum (OAM), a parameter that can only be measured by OAM radars.

To sum up, most algorithms focus on point targets. With respect to unresolvable extended target parameter estimation, the idea based on MLE does not require array

Manuscript received September 01, 2022.
*Corresponding author.

antennas, keeping antenna scanning, or prior information such as the SNR of the target. Hence, it has great potential for engineering applications. Nevertheless, the existing methods based on MLE represented by [8], have two common problems.

The first is a large amount of computation. With the increase of range cells number, the amount of computation for MLE increases exponentially [8]. In an ordinary wideband radar, a target may occupy dozens or even hundreds of range cells, resulting in too much computation to perform.

Second, there exists the risk of model mismatch. The derivation of the algorithms [8] is in accordance with statistical assumptions on echoes such as the Rayleigh distribution. Under the condition of narrowband (namely, low range resolution), each range cell contains a large number of scattering points. In other words, the distribution assumptions may hold. However, with the increase in radar bandwidth, the scattering points contained in the range cell are sharply reduced, and the distribution assumption can no longer hold [24,25]. Considering that the resolution of different wideband radars significantly varies, it is impossible to be described by a single statistical distribution. Therefore, the unresolved extended targets estimation methods based on distribution assumption may have model mismatch when applied to wideband radars.

In this paper, an algorithm based on wide-narrow band joint processing is proposed to estimate the parameters of the unresolvable extended target, so as to wrestle with the above problems.

Under high-resolution conditions, the range sampling points that only sample the echoes from resolvable parts of the unresolved targets (referred to as the resolvable target sampling points) are detected. These sampling points are adopted to estimate the parameters of each target. Subsequently, these parameters are applied to the MLE of unresolved targets under low-resolution conditions.

2. Signal modeling and parameter estimation

2.1 Wideband signal model and parameter estimation algorithm

As the model and processing algorithm of the elevation difference channel is the same as that of the azimuth difference channel, only the model and processing algorithm of the azimuth difference channel are described in this paper. In the wideband mode, the echo signals received by the radar sum and azimuth difference channels are comprised of channel I (in-phase component) and Q (quadrature component) signals. Assume that the amplitudes of each sampling point on the range profile are independent. If the unresolved targets are composed of N targets, and the sth target contains N_s scattering points, the sampling values of the four channel signals [5,8] can be expressed as

$$\begin{cases} s_i(j) = \sum_{s=1}^{N}\sum_{l=1}^{N_s} A_{sl}\cos(\phi_{sl})r(j\Delta t-\tau_{sl}) + n_{si}(j\Delta t) \\ s_q(j) = \sum_{s=1}^{N}\sum_{l=1}^{N_s} A_{sl}\sin(\phi_{sl})r(j\Delta t-\tau_{sl}) + n_{sq}(j\Delta t) \\ d_i(j) = \sum_{s=1}^{N}\sum_{l=1}^{N_s} A_{sl}\eta_s\cos(\phi_{sl})r(j\Delta t-\tau_{sl}) + n_{di}(j\Delta t) \\ d_q(j) = \sum_{s=1}^{N}\sum_{l=1}^{N_s} A_{sl}\eta_s\sin(\phi_{sl})r(j\Delta t-\tau_{sl}) + n_{dq}(j\Delta t) \end{cases} \tag{1}$$

where $s_i(j)$ and $s_q(j)$ denote the amplitude of the jth sampling point of the sum channels I and Q, respectively; $d_i(j)$ and $d_q(j)$ represent the amplitude of the jth sampling point of the azimuth difference channels I and Q, respectively; A_{sl} indicates the echo amplitude of the lth scattering point of the sth target; ϕ_{sl} signifies the phase of the echo from the lth scattering point of sth targets, which follows the uniform distribution between $(-\pi,\pi]$; $r(t)$ refers to the known matched filter response; Δt stands for the sampling period; n_{si} and n_{sq} express the noise amplitude after sampling of channels I and channel Q, respectively, and they are a Gaussian random process with mean value 0 and variance σ_Σ^2; n_{di} and n_{dq} denotes the noise amplitude of azimuth difference channels I and Q after sampling, respectively, following the Gaussian random process with mean value 0 and variance σ_Δ^2; τ_{sl} denotes the two-way delay of the radar signal detecting the lth scattering point of the sth target; η_s is the azimuth angle of the sth target. Then, the real part $y_R(j)$ and imaginary part $y_I(j)$ of the monopulse ratio at the jth sampling point are expressed as

$$\begin{cases} y_R(j) = \dfrac{d_i(j)s_i(j)+d_q(j)s_q(j)}{s_i(j)^2+s_q(j)^2} \\ y_I(j) = \dfrac{d_q(j)s_i(j)-d_i(j)s_q(j)}{s_i(j)^2+s_q(j)^2} \end{cases}. \tag{2}$$

In (2), $y_I(j)$ increases significantly in the presence of unresolved targets, and y_R is generally employed to estimate the angle $\theta = K_m y_R$ of the target, where K_m is a constant related to the antenna beamwidth. Unresolved targets cause angular glint, and the glint amplitude of the jth sampling point in the $k-n$ matched received echo pulse is denoted as

$$G_{k-n}(j) = {y_R}^{k-n}(j) - \bar{y}_R^k(j),\ \ n = 0,1,\cdots,K_0-1 \tag{3}$$

where

$$\bar{y}_R^k(j)=\sum_{n=0}^{K_0-1}{R_O}^{k-n}(j){y_R}^{k-n}(j)\Big/\sum_{n=0}^{K_0-1}{R_O}^{k-n}(j).$$

where K_0 is the number of pulses adopted to estimate $G(j)$.

The SNR of the jth sampling point is defined as

$${R_O}^k(j)=\frac{s_i^k(j)^2+s_q^k(j)^2}{\sigma_\Sigma^2}.$$

To sum up, $G(j)$ and $y_I(j)$ are the features to detect the existence of unresolved targets. In addition to the above two features, other effects caused by unresolved targets such as range jitter [26] and phase jitter [27] can also be utilized. The detection of unresolved targets requires a low correlation between echoes, which can be achieved through frequency hopping or experience replay [28]. The feature vector corresponding to the jth sampling point at time k is defined [6] as

$$\boldsymbol{x}_k^j=\left[x_k^1(j),x_k^2(j)\right]^{\mathrm{T}} \tag{4}$$

where $x_k^1(j)$ and $x_k^2(j)$ are calculated as

$$\begin{cases}x_k^1(j)=\boldsymbol{GRG}^{\mathrm{T}}\\ x_k^2(j)=\boldsymbol{Y_IRY_I}^{\mathrm{T}}\end{cases} \tag{5}$$

and

$$\boldsymbol{R}=\mathrm{diag}({R_O}^{k-K_0+1}(j),{R_O}^{k-K_0+2}(j),\cdots,{R_O}^k(j)), \tag{6}$$

$$\boldsymbol{G}=[\hat{G}_{k-K_0+1}(j),\hat{G}_{k-K_0+2}(j),\cdots,\hat{G}_k(j)], \tag{7}$$

$$\boldsymbol{Y_I}=[{y_I}^{k-K_0+1}(j),{y_I}^{k-K_0+2}(j),\cdots,{y_I}^k(j)]. \tag{8}$$

Under different radar bandwidths, the fluctuation probability distribution of echo amplitude varies, resulting in different probability distributions of $\boldsymbol{x}_k^j$. In this paper, Gaussian mixture model (GMM) is introduced to model the probability distribution of $\boldsymbol{x}_k^j$, so as to address $\boldsymbol{x}_k^j$ with different bandwidths. The GMM representation of $\boldsymbol{x}_k^j$ is

$$\begin{cases}p(\boldsymbol{x}_k^j)=\sum_{c=1}^{K_c}\omega_c\eta(\boldsymbol{x}_k^j;\boldsymbol{\mu}_c,\boldsymbol{\Sigma}_c)\\ \eta(\boldsymbol{x}_k^j;\boldsymbol{\mu}_c,\boldsymbol{\Sigma}_c)=\dfrac{1}{\sqrt{(2\pi)^{n_d}\boldsymbol{\Sigma}_c}}\exp\left(-\dfrac{1}{2}(\boldsymbol{x}_k^j-\boldsymbol{\mu}_c)^{\mathrm{T}}\boldsymbol{\Sigma}_c(\boldsymbol{x}_k^j-\boldsymbol{\mu}_c)\right)\end{cases} \tag{9}$$

where $p(\boldsymbol{x}_k^j)$ denotes the probability density function (PDF) of $\boldsymbol{x}_k^j$; K_c refers to the number of Gaussian components in GMM; ω_c indicates the weight of each component, satisfying $\sum_{j=1}^{K_c}\omega_c=1$; $\eta(\boldsymbol{x}_k^j;\boldsymbol{\mu}_c,\boldsymbol{\Sigma}_c)$ represents the PDF of the cth Gaussian component, in which $\boldsymbol{\mu}_c$ and $\boldsymbol{\Sigma}_c$ are its mean and variance, respectively; n_d signifies the dimension of the vector $\boldsymbol{x}_k^j$. There are mature algorithms for parameter estimation of GMM [29]. The Bayesian detector is designed as follows with the above model. Define the following events.

H_0: There are no unresolved targets echoes in the signal collected at the sampling point.

H_1: There are unresolved targets echoes in the signal collected at the sampling point.

Then, the Bayesian detector is

$$\frac{p\left(\boldsymbol{x}_k^j|\mathrm{H}_1\right)P(\mathrm{H}_1)(c_{10}-c_{11})}{p\left(\boldsymbol{x}_k^j|\mathrm{H}_0\right)P(\mathrm{H}_0)(c_{01}-c_{00})}\underset{\mathrm{H}_0}{\overset{\mathrm{H}_1}{\gtrless}}1 \tag{10}$$

where $p\left(\boldsymbol{x}_k^j|\mathrm{H}_1\right)$ and $p\left(\boldsymbol{x}_k^j|\mathrm{H}_0\right)$ indicate conditional PDFs of $\boldsymbol{x}_k^j$, respectively, corresponding to the output of GMM under the two conditions; $P(\mathrm{H}_1)$ and $P(\mathrm{H}_0)$ denote the prior probabilities of the occurrence of events H_1 and H_0, respectively, calculated following the prior information; c_{ij} expresses the cost constant, representing the cost when deciding event H_j is true while event H_i is true.

The resolvable target sampling points can be detected by using the above algorithm to detect the existence of unresolved targets for all sampling points in the target range profile. The serial number set of these sampling points in the target range profile is $E=\{e(i)|i=1,2,\cdots,N_e\}$, where N_e represents the number of sampling points detected as resolvable targets in the range profile. The K_0 echoes can be adopted to estimate the angle of the sampling point numbered $e(i)$:

$$\hat{\eta}_{e(i)}=\frac{\sum_{n=0}^{K_0-1}{R_O}^{k-n}[e(i)]\hat{\eta}^{k-n}[e(i)]}{\sum_{n=0}^{K_0-1}{R_O}^{k-n}[e(i)]} \tag{11}$$

and

$$\hat{\eta}^{k-n}[e(i)]=K_m{y_R}^{k-n}[e(i)]. \tag{12}$$

The angle estimates of the resolvable target sampling points from the same target are similar. This rule is employed in this paper to divide E into multiple subsets $\{T_1,T_2,\cdots,T_{N_T}\}$, where N_T denotes the number of resolvable targets, and each subset contains the number of resolvable target sampling points belonging to the same target; $|T_i|\geqslant 1$ $(i=1,2,\cdots,N_T)$ and $\bigcap_{k=1}^{N_T}T_k=\varnothing$.

Since the statistical distribution of $\hat{\eta}_{e(i)}$ is different under different bandwidths, the probability distribution of $\hat{\eta}_{e(i)}$ is modeled using GMM to ensure that the algorithm is suitable for various bandwidth conditions. The feature vector is defined as $\boldsymbol{x}_n^i=[\hat{\eta}_{e_0(1)},\hat{\eta}_{e_0(i)}]^{\mathrm{T}}$, where $1\leqslant n\leqslant N_T$ refers to the number of the target, $e_0(i)\in T_0$, and T_0 stands for the number set of sampling points to be divided. Noticeably, $\bigcup_{k=1}^{n-1}T_k\cup T_0=T$, where T_k signifies the serial number set of resolvable sampling points corresponding to the kth target. Define the following events.

H_0: The two sampling points corresponding to the fea-

ture vectors belong to the same target.

H_1: The two sampling points corresponding to the feature vector do not belong to the same target.

Then, the Bayesian detector is

$$\frac{p(\boldsymbol{x}_n^i|\mathrm{H}_1)P(\mathrm{H}_1)(c_{10}-c_{11})}{p(\boldsymbol{x}_n^i|\mathrm{H}_0)P(\mathrm{H}_0)(c_{01}-c_{00})} \underset{\mathrm{H}_0}{\overset{\mathrm{H}_1}{\gtrless}} 1. \tag{13}$$

The two conditional probability densities are the output of the GMM model under the condition that the two events are true, respectively. Similarly, Doppler, polarization, and other elements can be added to the feature vector to make use of more information. Given the target range profile P_{R}, the prior probability $P(\mathrm{H}_0) = P\left(\boldsymbol{x}_n^i \middle| P, \hat{\eta}_{e(1)}\right)$, $P(\mathrm{H}_1) = 1-P(\mathrm{H}_0)$ can be calculated. In the absence of target range profile prior information, $P(\mathrm{H}_0) = P(\mathrm{H}_1)$. For vector $\boldsymbol{x}_n^i$, if H_1 is true, $\hat{\eta}_{e(1)}$ and $\hat{\eta}_{e(i)}$ belong to different targets; otherwise, they belong to the same target. After traversing all elements of T_0 and completing the classification of all $e_0(i)$, the sampling point set T_n of the n targets can be obtained. T_n is removed from T_0 to obtain a new T_0. The steps above are repeated until $T_0 = \varnothing$, suggesting that the partitioning of set T is complete. The flow of the partitioning algorithm is illustrated in Fig. 1.

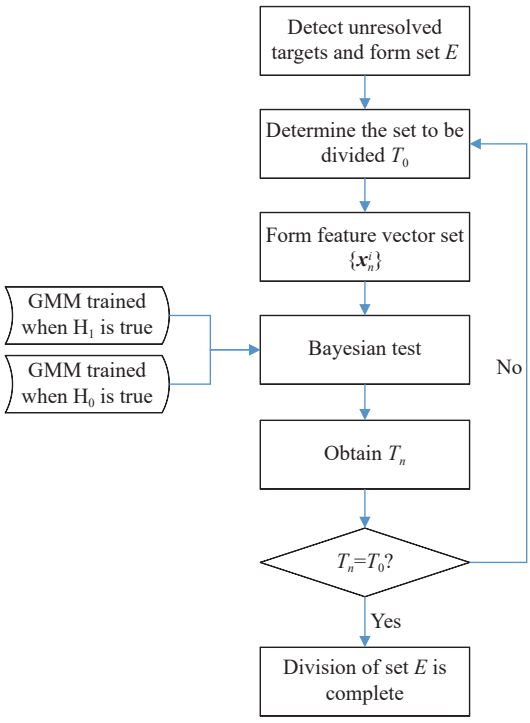

Fig. 1 Flow chart of set partitioning algorithm

The pseudocode for the wideband mode are shown in Algorithm 1.

Algorithm 1 Wideband mode

Function EstimateInWideBandMode($s_i^k, d_i^k, s_q^k, d_q^k, \sigma_\Sigma$)/

$y_R^k(j) := [d_i^k(j)s_i^k(j) + d_q^k(j)s_q^k(j)]/[s_i^k(j)^2 + s_q^k(j)^2]$;

$y_I^k(j) := [d_q^k(j)s_i^k(j) - d_i^k(j)s_q^k(j)]/[s_i^k(j)^2 + s_q^k(j)^2]$;

$R_O^k(j) := \left[s_i^k(j)^2 + s_q^k(j)^2\right]/\sigma_\Sigma^2$;

G_k:=Calculate_Angular_glint(y_R^k, R_O^k);

$\boldsymbol{R} = \mathrm{diag}(R_O^{k-K_0+1}(j), R_O^{k-K_0+2}(j), \cdots, R_O^k(j))$

$\boldsymbol{G} = [\hat{G}_{k-K_0+1}(j), \hat{G}_{k-K_0+2}(j), \cdots, \hat{G}_k(j)]$

$\boldsymbol{Y_I} = [y_I{}^{k-K_0+1}(j), y_I{}^{k-K_0+2}(j), \cdots, y_I{}^k(j)]$

$\boldsymbol{x}_k^j = \left[\boldsymbol{GRG}^{\mathrm{T}}, \boldsymbol{Y_I R Y_I}^{\mathrm{T}}\right]$;/*feature vector*/

c_{10}:=1; c_{11}:=0; c_{01}:=1; c_{00}:=0;

For j: = 1 to number of sampling points{

PH0 := $P(\boldsymbol{x}_k^j, \mathrm{H}_0)$;/*The likelihood of x coming from resolvable targets, output of GMM*/

PH1 := $P(\boldsymbol{x}_k^j, \mathrm{H}_1)$;

IF (PH0/PH1)$*(c_{01}/c_{10}) > 1$ Then

Add the data of the jth sampling point to **Resolvable sample**

/}i: = 1;

WHILE IsNotEmpty(**ResolvableSample**){

$\boldsymbol{T}(i)$.**Element**:=**ResolvableSample**(1);

Remove **ResolvableSample**(1) from **ResolvableSample**;

For j: = 1 to number of elements in **ResolvableSample**{

x:=[$\boldsymbol{T}(i)$.**Element**.Angle, **ResolvableSample**(j).Angle];

PH0 := $P(\boldsymbol{x}, \mathrm{H}_0)$;/*The two sample points belong to the same target, output of GMM*/

PH1 := $P(\boldsymbol{x}, \mathrm{H}_1)$;

IF PH0/PH1 > 1 Then{

Move **ResolvableSample**(j) from **ResolvableSample** to $\boldsymbol{T}(i)$; /}

/} $i := i + 1$;

/}

For i := 1 to number of elements in $\boldsymbol{T}$ {

Angle(i):=EstimateAngle($\boldsymbol{T}(i)$) /}

ResolvableTargetNumber=i;

OUTPUT ResolvableTargetNumber, **Angle**

2.2 Narrowband signal model and parameter estimation algorithm

The target parameter estimation under narrowband mode is based on the maximum likelihood estimation algorithm proposed in [7]. Specifically, part of the parame-

ters estimated in advance under the wideband mode are employed to lessen the computation amount and improve the estimation accuracy. Considering that the high-resolution range profile (HRRP) of the combination comprised of unresolved targets in wideband mode has been obtained, the radial size of the combination can be estimated by counting the number of sampling points on its HRRP. With a 100 MHz bandwidth mode as an example, if an HRRP of unresolved target combination contains 30 sampling points, the radial size of the combination is $70\times1.5=45$ m, where 1.5 m is the range resolution. As the range resolution of 2.5 MHz bandwidth is 60 m, choosing 2.5 MHz or lower bandwidth in narrowband mode can guarantee that the echoes of the combination are located in a single true location, that is, located between the two adjacent range profile sampling points.

As illustrated in Fig. 2, t is defined as the distance from sampling point 1 to the true location of the target, and the matched filter response can be simplified as $r(t)=1-\dfrac{t}{\Delta t}$ $(0\leqslant t\leqslant\Delta t)$. x denotes the real amplitude of the target echo, and $\alpha=\dfrac{t}{\Delta t}$. Hence, the target echo amplitudes obtained at the two sampling points are exhibited in Fig. 2.

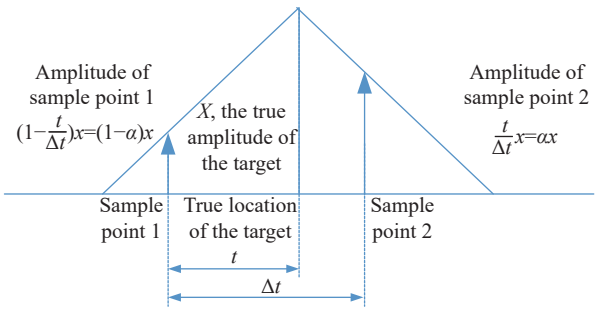

Fig. 2 Signal model for narrowband mode

Under this narrow band condition, the I-channel signal model of the sum channel and azimuth difference channel is

$$\begin{cases} s_{i1}(j)=\sum\limits_{s=1}^{N}(1-\alpha_s)A_s(j)\cos[\phi_s(j)]+n_{si}(j) \\ s_{i2}(j)=\sum\limits_{s=1}^{N}\alpha_s A_s(j)\cos[\phi_s(j)]+n_{si}(j) \\ d_{hi1}(j)=\sum\limits_{s=1}^{N}(1-\alpha_s)A_s(j)\eta_{hs}\cos[\phi_s(j)]+n_{dhi}(j) \\ d_{hi2}(j)=\sum\limits_{s=1}^{N}\alpha_s A_s(j)\eta_{hs}\cos[\phi_s(j)]+n_{dhi}(j) \end{cases} \tag{14}$$

where j represents the serial number of the data collection period, which can be the pulse repetition interval, coherent processing interval, or other periods. The condition for selecting the data collection period aims to ensure statistical independence among the sampled data. Additionally, $s_{i1}(j)$ and $s_{i2}(j)$ indicate the amplitudes of sampling point 1 and sampling point 2 of channel I obtained by the jth sampling, respectively; $d_{hi1}(j)$ and $d_{hi1}(j)$ express the azimuth difference I amplitude of sampling point 1 and sampling point 2 obtained from the jth sampling, respectively. The channel noise $n_{si}(j)$ is a Gaussian random process with mean 0 and variance $\sigma^2_{\Sigma_{nb}}$, and $n_{dhi}(j)$ is a Gaussian random process with mean 0 and variance $\sigma^2_{\Delta_{nb}}$. $A_s(j)$ denotes the signal amplitude of target s at the jth sampling point. In the narrowband mode, all scattering points of the target are located in a radar range cell, and A_s follows the Rayleigh distribution with parameter σ_s. Under the assumption that phase $\phi_s(j)$ follows a uniform distribution, $A_s(j)\cos[\phi_s(j)]$ is a Gaussian random variable with mean 0 and variance σ_s^2 [8]. Given that the variance of the noise can be easily obtained, the variance $\sigma^2_{\Sigma_{nb}}=\sigma^2_{\Delta_{nb}}=1$ of the sum channel and the difference channel can be assumed. On this basis, the sampled values of each channel are the weighted sum of Gaussian distributions with mean 0 and follow the Gaussian distribution with mean 0.

The two channels I and Q are independent of each other. Consequently, the model only comprises the sum difference channel I sampling of the two sampling points, and the Q sampling can be regarded as the data collected in another data collection period. Therefore, M data collection periods indicate that $2M$ groups of data can be obtained.

Then, the observation vector is defined as

$$\boldsymbol{z}(j)=[s_{i1}(j),s_{i2}(j),d_{hi1}(j),d_{hi2}(j),d_{vi1}(j),d_{vi2}(j)]^{\mathrm{T}}. \tag{15}$$

The observation vector $\boldsymbol{z}$ only contains the amplitudes of the I signal of the sum and difference channels, and the amplitudes of the Q signals corresponding to each channel can be viewed as another independent observation.

With (15), the parameter vector to be estimated is

$$\boldsymbol{\theta}=[\sigma_1,\alpha_1,\eta_{h1},\eta_{v1},\sigma_2,\alpha_2,\eta_{h2},\eta_{v2},\cdots,\sigma_N,\alpha_N,\eta_{hN},\eta_{vN}]^{\mathrm{T}}. \tag{16}$$

Additionally, the angle estimation $\{\hat{\eta}_1,\hat{\eta}_2,\cdots,\hat{\eta}_{N_T}\}$ of the resolvable target has been completed under the condition of high resolution. Therefore, the actual number of parameters to be estimated is $|\boldsymbol{\theta}|-N_T$. The conditional probability density function of $\boldsymbol{z}(j)$ regarding $\boldsymbol{\theta}$ is a multi-dimensional Gaussian PDF with mean $\boldsymbol{z}(j)$ and covariance matrix $\boldsymbol{R}=\mathrm{E}[\boldsymbol{z}\boldsymbol{z}^{\mathrm{T}}]$[30].

$$\boldsymbol{R}=\sum_{s=1}^{N}\sigma_s^2\begin{bmatrix}(1-\alpha_s)^2 & (1-\alpha_s)\alpha_s & (1-\alpha_s)^2\eta_{hs} & (1-\alpha_s)\alpha_s\eta_{hs} & (1-\alpha_s)^2\eta_{vs} & (1-\alpha_s)\alpha_s\eta_{vs}\\ (1-\alpha_s)\alpha_s & \alpha_s^2 & (1-\alpha_s)\alpha_s\eta_{hs} & \alpha_s^2\eta_{hs} & (1-\alpha_s)\alpha_s\eta_{vs} & \alpha_s^2\eta_{vs}\\ (1-\alpha_s)^2\eta_{hs} & (1-\alpha_s)\alpha_s\eta_{hs} & (1-\alpha_s)^2\eta_{hs}^2 & (1-\alpha_s)\alpha_s\eta_{hs}^2 & (1-\alpha_s)^2\eta_{hs}\eta_{vs} & (1-\alpha_s)\alpha_s\eta_{hs}\eta_{vs}\\ (1-\alpha_s)\alpha_s\eta_{hs} & \alpha_s^2\eta_{hs} & (1-\alpha_s)\alpha_s\eta_{hs}^2 & \alpha_s^2\eta_{hs}^2 & (1-\alpha_s)\alpha_s\eta_{hs}\eta_{vs} & \alpha_s^2\eta_{hs}\eta_{vs}\\ (1-\alpha_s)^2\eta_{vs} & (1-\alpha_s)\alpha_s\eta_{vs} & (1-\alpha_s)^2\eta_{hs}\eta_{vs} & (1-\alpha_s)\alpha_s\eta_{hs}\eta_{vs} & (1-\alpha_s)^2\eta_{vs}^2 & (1-\alpha_s)\alpha_s\eta_{vs}^2\\ (1-\alpha_s)\alpha_s\eta_{vs} & \alpha_s^2\eta_{vs} & (1-\alpha_s)\alpha_s\eta_{hs}\eta_{vs} & \alpha_s^2\eta_{hs}\eta_{vs} & (1-\alpha_s)\alpha_s\eta_{vs}^2 & \alpha_s^2\eta_{vs}^2\end{bmatrix}+$$
$$\operatorname{diag}(\sigma_{\Sigma_{nb}}^2,\sigma_{\Sigma_{nb}}^2,\sigma_{\Delta_{nb}}^2,\sigma_{\Delta_{nb}}^2,\sigma_{\Delta_{nb}}^2,\sigma_{\Delta_{nb}}^2) \tag{17}$$

The final covariance matrix $\boldsymbol{R}$ is obtained by substituting $\{\hat{\eta}_1,\hat{\eta}_2,\cdots,\hat{\eta}_{N_T}\}$ into the above equation. Owing to the independence of M data, the likelihood function of the observation vector can be written as

$$L(\boldsymbol{\theta})=\prod_{j=1}^{M}((|2\pi\boldsymbol{R}|)^{-1/2}\exp[-0.5z(j)^{\mathrm{T}}\boldsymbol{R}^{-1}z(j)]). \tag{18}$$

The estimation of parameter $\boldsymbol{\theta}$ is achieved by solving the constrained maximum likelihood estimation [7].

$$\hat{\boldsymbol{\theta}}=\arg\max_{\boldsymbol{\theta}}\{L(\boldsymbol{\theta})\} \tag{19}$$

The constraint condition is

$$\begin{cases}\sigma_s^2\geqslant 0\\ 0\leqslant\alpha_s\leqslant 1\\ -1\leqslant\eta_{hs}\leqslant 1\\ -1\leqslant\eta_{vs}\leqslant 1\end{cases}.$$

The number of targets is estimated by the MDL criterion [7]. In the calculation of MDL length, the PTE algorithm should traverse possible target numbers by assuming $N=1,2,3,4,\cdots$. When $N>1$, under each of the assumptions, an MLE of parameters needs to be solved, which requires a large amount of computation. In the proposed algorithm, there are N_T resolvable targets detected in wideband mode. Hence, the traversal of N starts at N_T instead of 1, contributing to the reduced computation.

The workflow of the proposed algorithm is illustrated in Fig. 3.

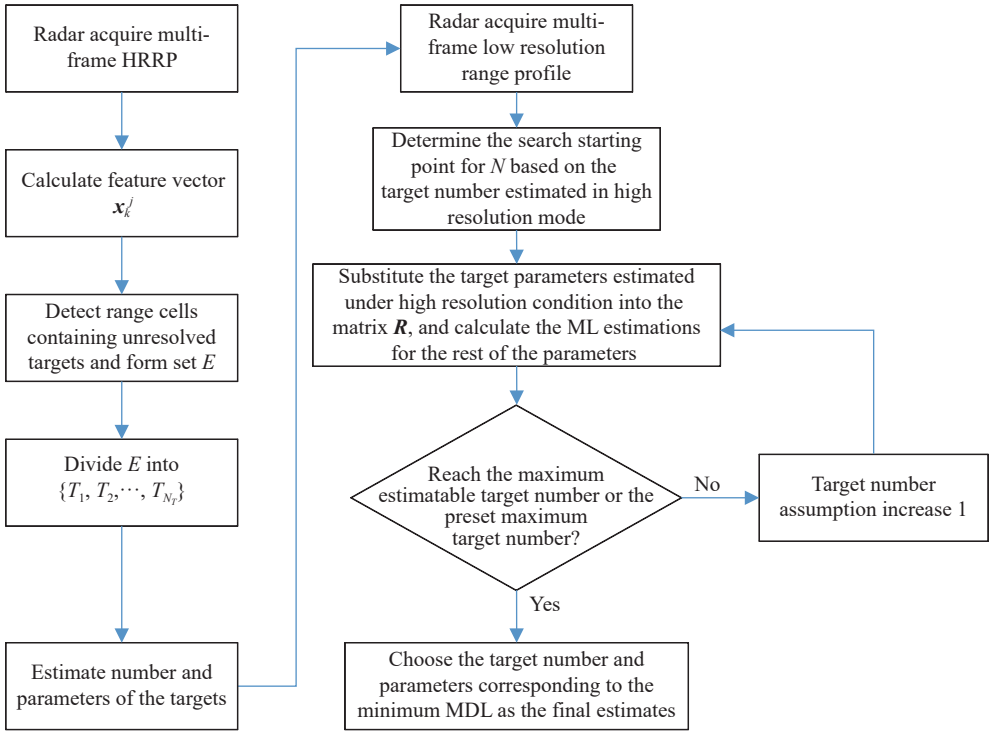

Fig. 3 Flow chart of the proposed algorithm

The pseudocode for the narrowband mode is shown in Algorithm 2.

Algorithm 2 Narrowband mode

Function EstimateInNarrowBandMode(ResolvableTargetNumble, **Angle**)

invR:=inv(***R***); /*Find the inverse matrix of ***R****/

FOR j := 1 to MLowResolution{

estKsum:=**estKsum** + zz^{T} /}/*MLowResolution is the number of pulses used for estimation.*/

LL:=−ln(det(***R***))-trace(invR***estKsum**);/*Log-Likelihood function of the observation vector.*/

N_T :=ResolvableTargetNumber/*Minimum target number.*/

k:=N_T;

WHILE TRUE {

Substitute **Angle** to LL

$\boldsymbol{\theta}(k)$:=MLE(LL);/*Estimate parameters by MLE.*/

MDL(k)=CalculateMDL($\boldsymbol{\theta}$,k);

IF $k-N_T$ >1 AND MDL(k)>MDL(k−1) THEN {

BREAK;

k:=k+1:/}

/} OUTPUT $\boldsymbol{\theta}(k-1)$;

The advantages of this idea are detailed as follows.

Firstly, it avoids the risk of model mismatch caused by the diversity of radar bandwidths. Secondly, the proposed algorithm detects the resolvable target sampling point in wideband mode, estimates part of the target parameters, and utilizes the estimates as prior information in the MLE. In this way, the advantage of high resolution can be used to improve the estimation performance of the algorithm for the unresolved target. Thirdly, the MLE is only solved under the narrowband mode to considerably reduce the computation.

For applications, the signal required by the wide-narrowband joint processing can be easily obtained. Ordinary wideband radar can change the signal bandwidth, while synthetic wideband radar can employ the wide-narrowband joint processing without changing the bandwidth of the transmitted signal because its sub-pulses are in narrowband.

3. Experiment and analysis

The MRSP-E algorithm [8] is the latest algorithm applicable to the same scenario as the proposed algorithm. Thus, it is used as the benchmark in the simulation experiment. Additionally, as the PTE algorithm [7] is similar to the proposed algorithm in narrowband mode, it is also compared with the proposed algorithm to more comprehensively analyze the characteristics of the proposed algorithm.

3.1 Experiment 1: comparison of estimation accuracy and computation amount

In this experiment, the proposed algorithm is compared with the MRSP-E algorithm and the PTE estimation algorithm. The experimental scenarios and parameters are set as follows.

3.1.1 Scenario setting

(i) In the scenario, a monopulse radar working at 10 GHz has a signal bandwidth of 30 MHz with a range resolution of 5 m under wideband mode, as well as a signal bandwidth of 10 MHz with a range resolution of 15 m under narrow band mode.

(ii) There are two targets, where Target 1 contains two scattering points, and Target 2 contains one scattering point. The two targets are located within the 3 dB beam of the radar. Specifically, they are unresolved in azimuth.

(iii) The layout of scattering points in range dimension in the wideband mode is illustrated in Fig. 4. One of the scattering points of Target 1 is located in the same range cell as Target 2, and the two scattering points are unresolved. Then, the parameter to be estimated for the l scattering points of the Target s is (α_{sl},η_{hsl}), where $\alpha_{sl}\in[0,1]$ represents the distance from the scattering points to the starting sampling point of the range cell and normalized by the length of the range cell. The azimuth is normalized by the beam of 3 dB, $\eta_{hsl}\in[-1,1]$. In the simulation, the variance of the sum channel noise σ_{Σ} and difference channel noise σ_{Δ} are both set to 1. Thus, σ_{sl}^2 is considered the SNR of the echo of these scattering points. The true values of the two scattering points parameters of Target 1 are (0.4,−0.1) and (0.8,−0.1). The true values of the scattering point parameters of Target 2 are (0.3,0.7).

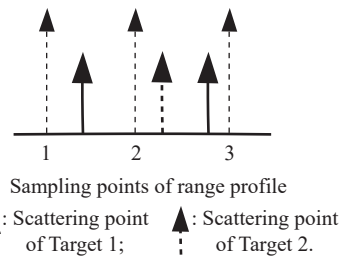

Fig. 4 Scattering point layout of two targets in wideband mode

(iv) In the narrowband mode, the parameter to be estimated for target s is (α_s,η_{hs}), where $\alpha_s\in[0,1]$ and $\eta_{hs}\in[-1,1]$. The variance of sum channel noise $\sigma_{\Sigma_{nb}}$ and difference channel noise $\sigma_{\Delta_{nb}}$ are both set to 1. The true value of the Target 1 parameters is (0.55, −0.1), and the true value of the Target 2 parameters is (0.325,0.7). The two targets are located in the main beam in azimuth and one range cell in range, suggesting that they are unre-

solved targets.

(v) All programs run on the same computer configured with Intel Core i7-4790K@4.00 GHz, 8 GB RAM.

3.1.2 Simulation results

The MRSP-E algorithm is adopted to estimate (α_{sl},η_{hsl}) of each scatter point under wideband mode. Regarding this algorithm, one estimation is completed using 33 independent pulses ($N_d = 33$). The echo amplitude variance of each scattering point is set equal and $\sigma_{sl} = 10$ (corresponding to the SNR of 20 dB). The PTE algorithm is adopted to estimate (α_s,η_{hs}) of each target under the narrowband mode, with $N_d = 33$, $\sigma_s = 10$. The proposed algorithm is adopted to estimate (α_s,η_{hs}), with $N_d = 33$, $\sigma_s = 10$. The cost constant of the Bayesian detector is set to 1, and the number of components of the GMM model is 10. In addition, 1 000 Monte Carlo simulations are performed for each of the three algorithms.

The estimation results of the proposed algorithm and the PTE algorithm are depicted in Fig. 5. In Fig. 5, black points indicate the result of the proposed algorithm, and gray points represent the result of the PTE point estimation algorithm; the true value of the target parameters are $\alpha_1 = 0.55$, $\eta_{h1} = -0.1$, $\alpha_2 = 0.325$, and $\eta_{h2} = 0.7$. The estimation results of the MRSP-E algorithm are exhibited in Fig. 6. The true value of scattering point parameters are $\alpha_{11} = 0.4$, $\eta_1 = -0.1$, $\alpha_{12} = 0.8$, $\alpha_{21} = 0.3$, and $\eta_2 = 0.7$.

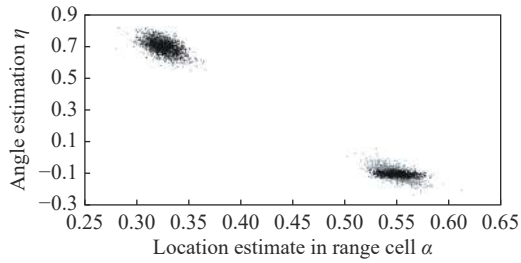

Fig. 5 Estimation results of two algorithms

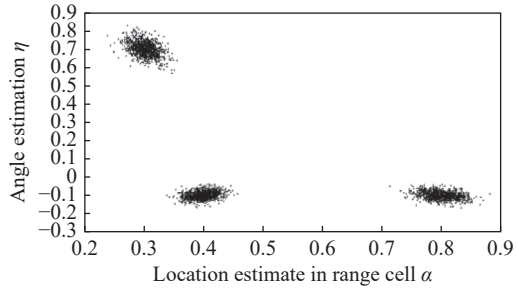

Fig. 6 Estimation results of MRSP-E algorithm

Fig. 5 reveals that the dispersion degree of the estimation result of Target 1 by the proposed algorithm is smaller than that of the PTE algorithm. Particularly, the estimation of η_1 by the proposed algorithm is more concentrated and closer to the true value. This is in that the proposed algorithm estimates η_1 by using the resolvable target sampling points under wideband modes, and the estimation performance of the proposed algorithm on other parameters is slightly improved by substituting the estimation into the solution of MLE. The root mean square errors (RMSEs) of the results of the proposed algorithm and the PTE algorithm are listed in Table 1. The RMSE of the proposed algorithm for the estimation of four parameters is less than or equal to that of the PTE algorithm. The RMSE of MRSP-E estimation results relative to the true value are provided in Table 2. It can be observed that the RMSE results are greater than those of the proposed algorithm.

Table 1 Comparison of RMSEs between the proposed algorithm and PTE algorithm

Algorithm	α_1	η_{h1}	α_2	η_{h2}
Proposed algorithm	0.010 3	0.012 2	0.010 3	0.037 2
PTE algorithm	0.010 3	0.040 3	0.012 9	0.037 4

Table 2 RMSE of MRSP-E algorithm results

Paremeter	RMSE
α_{11}	0.017 7
η_{h11}	0.020 3
α_{12}	0.022 8
η_{h12}	0.020 3
α_{21}	0.016 7
η_{h21}	0.039 1

The comparison of the computation time of the three algorithms after 1 000 times of Monte Carlo simulation is presented in Fig. 7. The compute time of the proposed algorithm is the shortest since the proposed algorithm estimates η_1 from the resolvable target sampling points under wideband mode, which lessens the number of parameters to be estimated in the MLE and significantly reduces the computation.

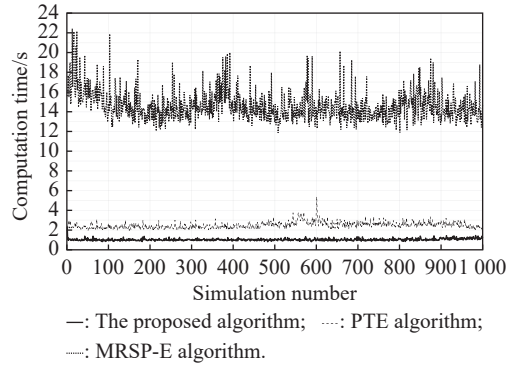

Fig. 7 Comparison of computation time of the three algorithms

3.2 Experiment 2: factors affecting estimation accuracy and computation amount

This experiment analyzes the influence of target echo SNR σ and pulse number N_d on the performance of the

proposed algorithm and the PTE algorithm. Let N_d increase from 6 to 33 with a step value of 3 and performs 1 000 Monte Carlo simulations for each step. The SNR of the scattering points and the target are set to 20 dB, and the other parameters are the same as in Experiment 1. When the number of targets is assumed to be equal to the true value of the number of targets, the RMSE of the estimation results of the two algorithms are illuminated in Fig. 8 and Fig. 9. As revealed in the figures, the RMSE of the two algorithms gradually decreases with the increase of N_d because more N_d brings more information. In Fig. 8, the two algorithms have the same performance, because the parameter α estimated in wideband mode cannot be used in narrowband mode, therefore, the two algorithms have the same information. In Fig. 9, the RMSE of Target 1 angle estimate yielded by the proposed algorithm is lower compared to the PTE algorithm. This is because that the proposed algorithm has estimated the Target 1 angle with high accuracy in wideband mode beforehand, while the PTE algorithm cannot estimate parameters in wideband mode.

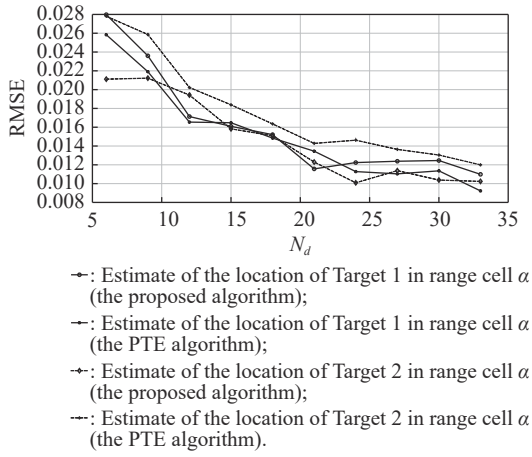

Fig. 8 RMSE of position parameter α estimation in range cell of the two algorithms

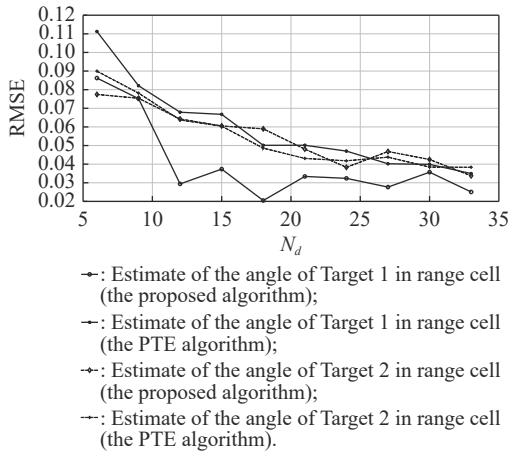

Fig. 9 RMSE of angel parameter η estimation of the two algorithms

The comparison of the operation time of the two algorithms is illustrated in Fig. 10. Under all N_d, the compute time of the proposed algorithm is less than that of the PTE algorithm.

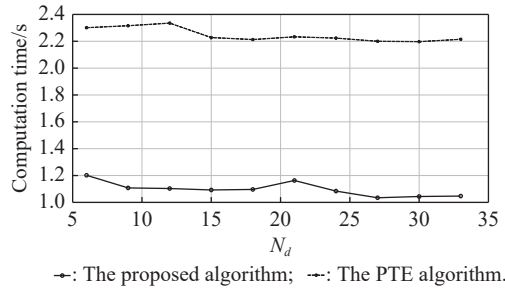

Fig. 10 Comparison of computation time v.s. N_d of the two algorithms

The SNR is set to increase from 13 to 31 with a step value of 2, and 1 000 Monte Carlo simulations are performed for each step. N_d is set to 33, and the remaining parameters are the same as those in Experiment 1. The RMSE of angle estimates are demonstrated in Fig. 11. As SNR increases, the RMSE of the angle of the two algorithms decreases. Moreover, the RMSE of Target 1 angle estimate yielded by the proposed algorithm is lower than that of the PTE algorithm. This is because that the proposed algorithm has estimated the Target 1 angle with high accuracy in wideband mode beforehand, while the PTE algorithm cannot estimate parameters in wideband mode. When SNR is higher than 28 dB, the two algorithms have the same performance.

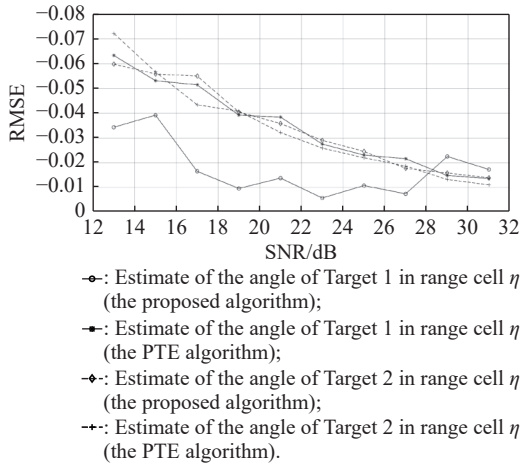

Fig. 11 Comparison of angel estimation RMSE of the two algorithms

The comparison of the operation time of the two algorithms is depicted in Fig. 12. As SNR increases, the computation time of the two algorithms increases. Moreover,

the computation time of the proposed algorithm is less than that of the PTE algorithm under each SNR.

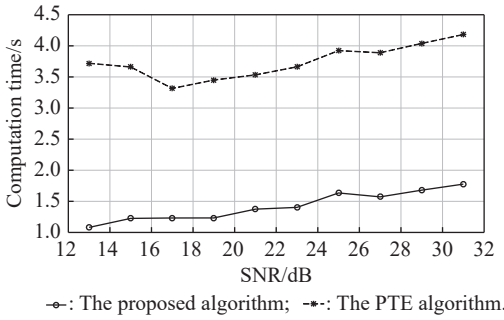

Fig. 12 Comparison of computation time v.s. SNR of the two algorithms

To sum up, the proposed algorithm has a lower computation amount and higher estimation accuracy compared with the PTE algorithm.

3.3 Experiment 3: comparison in an electromagnetic simulation scenario

The unresolved targets by electromagnetic scattering simulation are simulated to test the performance of the proposed algorithm in a more realistic scenario.

In this scenario, a monopulse radar working at 10 GHz has a signal bandwidth of 100 MHz with a range resolution of 1.5 m under the wideband mode, as well as a signal bandwidth of 1 MHz with a range resolution of 150 m under narrow band mode. The beamwidth of the radar is 7°. The radar is tracking a combination comprised of two unresolved targets, as illustrated in Fig. 13.

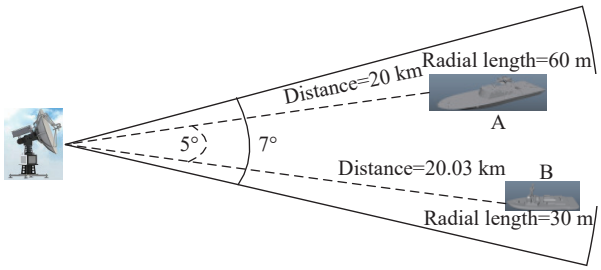

Fig. 13 Position of the ships

Ship A and Ship B are 60 m and 30 m long, respectively, and the radial distance relative to the radar is 20 km and 20.03 km, respectively. In other words, the two targets partially overlap in the radial distance, and the overlapping part of the radar is unresolvable in the radial distance. Additionally, the azimuth angle of Ship A relative to the radar is 3°, the azimuth angle of Ship B relative to the radar is −2°, and the azimuth angle of the two targets is about 0.7 times the width of the radar beam 7°, rendering the two targets unresolvable in azimuth.

The HRRP of Ship A, Ship B, and the combination of the unresolved targets is displayed in Fig. 14, Fig. 15, and Fig. 16, respectively. In the HRRP figures, the ordinate represents the relative amplitude and has no physical unit; the abscissa is the serial number of each point in the HRRP, which does not represent target absolute radial distance, but has a linear relationship with the radial distance, that is, for 1 MHz HRRP, the radial distance difference between two adjacent points is 150 m, while for 100 MHz HRRP, the radial distance difference between two adjacent points is 1.5 m.

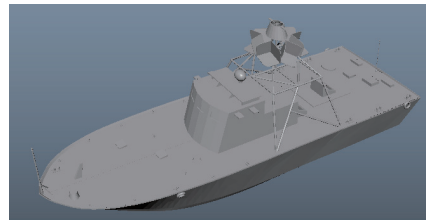

(a) 3D model of the target

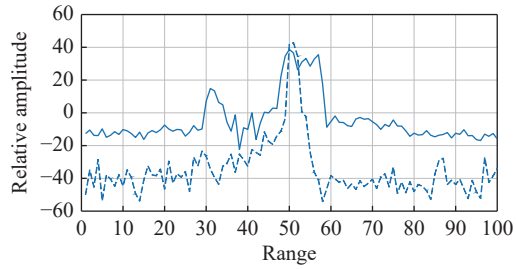

---: HRRP of 1 MHz mode; —: HRRP of 100 MHz mode.

(b) HRRP at 1 MHz and 100 MHz bandwidth

Fig. 14 HRRP Ship A model and its HRRP

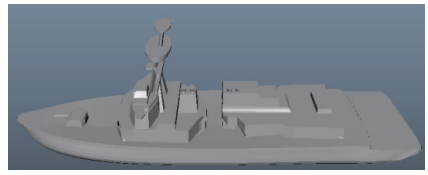

(a) 3D model of the target

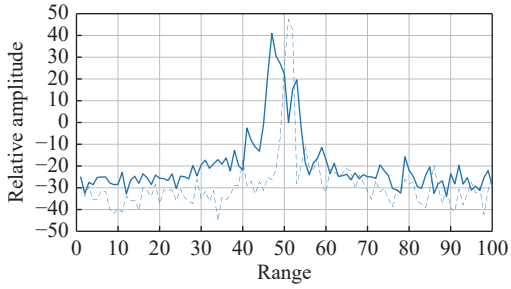

---: HRRP of 1 MHz mode; —: HRRP of 100 MHz mode.

(b) HRRP at 1 MHz and 100 MHz bandwidth

Fig. 15 HRRP Ship B model and its HRRP

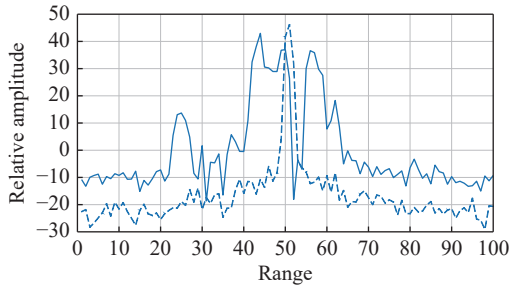

Fig. 16 HRRP in the sum channel of the unresolved targets combination in 1 MHz and 100 MHz bandwidths

The fluctuation of echoes in wideband mode and narrowband mode follows bimodal distribution and Rayleigh distribution, respectively. In addition, 1 000 HRRPs of the unresolved targets combination are generated as test data.

Since the target HRRP contains much more than three sampling points in wideband mode, the computation of the MRSP-E algorithm increases exponentially and cannot be calculated by a computer. Therefore, the proposed method and the PTE algorithm are compared regarding the performance in this experiment. According to the scenario settings, if the main beam range $[-3.5^\circ, 3.5^\circ]$ is mapped to $[-1,1]$, the true azimuth values of A and B can be expressed as $\eta_{\mathrm{A}} = 3/3.5 = 0.86$ and $\eta_{\mathrm{B}} = -(2/3.5) = -0.57$, respectively. Then, the estimation accuracy of the two algorithms will be evaluated with this value as the true value.

The pulse number parameter is set to $N_d = 33$ for the two algorithms, and the other parameters are the same as in Experiment 1.

The proposed algorithm firstly detects the sampling points of the resolved parts by test statistics x_k^1 and x_k^2, which are calculated by $\boldsymbol{G}$, $\boldsymbol{Y_I}$, and $\boldsymbol{R}$. The x_k^2 of HRRP is presented in Fig. 17. It can be suggested that x_k^2 of the sampling points of the resolved parts (points 24 to 40 and 60 to 64) is low, while x_k^2 of the sampling points of the unresolved parts (points 41 to 59) and noise is high.

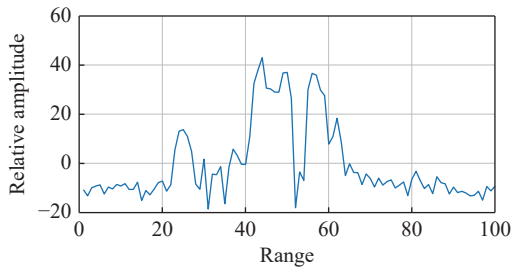

(a) HRRP in the sum channel of the unresolved targets combination in 100 MHz bandwidth

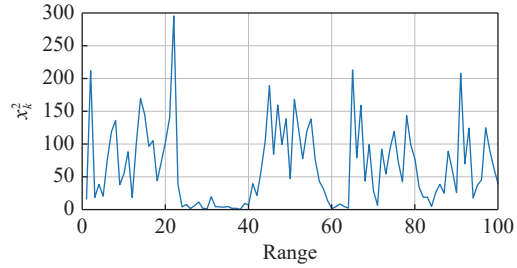

(b) x_k^2 of the HRRP

Fig. 17 HRRP of unresolved targets and the corresponding x_k^2

Afterwards, the sampling points of the resolved parts are detected, and points 24 to 40 and 60 to 64 are divided into two clusters. The azimuths of the two targets are measured by a common monopulse algorithm [31]. Subsequently, the azimuths are employed as the start point of MLE search in narrowband. In some HRRPs, sampling points of unresolved parts are detected, resulting in the relatively lower accuracy of azimuth measurement in the corresponding HRRP. The measured azimuths are then used as the start search point parameters of MLE in narrowband. However, the PTE algorithm, which runs on narrowband data, has no a priori information. Hence, the start search point parameters of MLE are set to 0 s. The azimuth estimation of the two algorithms is depicted in Fig. 18. In Fig. 18, black points are the result of the proposed algorithm, and gray points are the result of the PTE algorithm; the true values of the target parameters are $\alpha_1 = 0.43$, $\eta_{h1} = -0.57$, $\alpha_2 = 0.23$, and $\eta_{h2} = 0.86$.

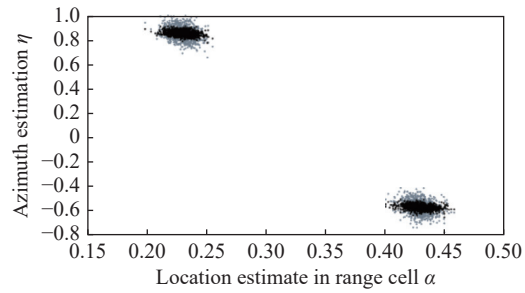

Fig. 18 Estimation results of two algorithms

The RMSE of the two algorithm's azimuth estimates are listed in Table 3.

Table 3 Comparison of azimuth estimation RMSEs of the proposed algorithm and PTE algorithm with the true value being 0.86 and −0.57

Algorithm	RMSE
The proposed algorithm	0.023 6
PTE algorithm	0.049 0

As shown in Fig.18 and Table 3, the RMSE of the proposed algorithm estimates is smaller since the proposed algorithm detects the resolvable parts under wideband modes, measures the angle of the two targets with these parts, and adopts the measurements for MLE under narrowband.

4. Conclusions

In this paper, a parameter estimation algorithm for unresolved targets is proposed based on wideband and narrowband joint processing. The simulation experiments verifies the effectiveness of the proposed algorithm. Compared with the MRSP-E algorithm and point estimation algorithm, the proposed algorithm has a lower computational cost and higher estimation accuracy.

Additionally, the proposed algorithm avoids model mismatch in wideband modes. It is more suitable for wideband radar with various kinds of resolution compared with the existing algorithms.

Finally, the proposed algorithm, though designed for wideband radar, is also applicable to other radars with high-resolution capability in time, frequency, polarization, and other domains.

References

[1] MA J Z, SHI L F, XU Z H, et al. Overview of multi-source parameter estimation and jamming mitigation for monopulse radars. Journal of Radars, 2019, 8(1): 125–139.

[2] BLAIR W D, BRANDT-PEARCE M. Unresolved Rayleigh detection using monopulse measurements. IEEE Trans. on Aerospace and Electronic Systems, 1998, 34(2): 543–552.

[3] LI C W, WANG H Q, LI X, et al. Study on the detection of the multiple unresolved targets. Journal of Systems Engineering and Electronics, 2005, 16(2): 295–300.

[4] YANG Y, FENG D J, ZHANG W M, et al. Detection of chaff centroid jamming aided by GPS/INS. IET Radar, Sonar & Navigation, 2013, 7(2): 130–142.

[5] GLASS J D, BLAIR W D. Detection of unresolved Rayleigh targets using adjacent bins. Proc. of the IEEE Aerospace Conference, 2016. DOI: 10.1109/AERO.2016.7500875.

[6] TSAI T Y, LIAO Z Q, DING Z Q, et al. Detection of unresolved targets for wideband monopulse radar. Sensors, 2019, 19(5): 1084.

[7] ZHANG X, WILLETT P K, BAR-SHALOM Y. Monopulse Radar detection and localization of multiple unresolved targets via joint bin Processing. IEEE Trans. on Signal Processing, 2005, 53(4): 1225–1236.

[8] ZHANG X, WILLETT P, BAR-SHALOM Y. Detection and localization of multiple unresolved extended targets via monopulse radar signal processing. IEEE Trans. on Aerospace and Electronic Systems, 2005, 45(2): 455–472.

[9] YANG Y, LI Y Y. A maximum likelihood extractor for forward-looking imaging of multiple unresolved targets in monopulse radar. Proc. of the CIE International Conference on Radar, 2016. DOI: 10.1109/RADAR.2016.8059347.

[10] YUAN H, WANG C Y, AN L, et al. Monopulse joint parameter estimation of multiple unresolved targets within the radar beam. Proc. of the IOP Conference Series Earth and Environmental Science, 2017, 69(1): 012155.

[11] WANG J, YAO J, QIAO X L. A practical approach of monopulse DOA estimation for multiple unresolved targets. Proc. of the IET International Radar Conference, 2009. DOI: 10.1049/cp.2009.0427.

[12] MA Y G, ZENG Y H, SUN S M. A deep learning based super resolution DoA estimator with single snapshot MIMO radar data. IEEE Trans. on Vehicular Technology, 2022, 71(4): 4142–4155.

[13] LIANG C, LIU A, YANG Q. DOA estimation using an extended spatial smoothing with coprime MIMO radar. Proc. of the IET International Radar Conference, 2021. DOI: 10.1049/icp.2021.0638.

[14] DONG F B, JIANG Y, LIU J, et al. Experimental study on the performance of DOA estimation algorithm using a coprime acoustic sensor array without a priori knowledge of the source number. Applied Acoustics, 2022, 186: 108502.

[15] CAO C H, ZHAO Y B, PANG X J, et al. A method based on Chinese remainder theorem with all phase DFT for DOA estimation in sparse array. Journal of Systems Engineering and Electronics, 2020, 31(1): 1–11.

[16] SAKAMOTO T. Generating a super-resolution radar angular spectrum using physiological component analysis. IEICE Communications Express, 2021, 10(10): 780–785.

[17] CHEN F, GUI C Y, MO S Q. Eigenvalue-based super-resolution DOA algorithm for arbitrary arrays. Applied Acoustics, 2021, 181: 108106.

[18] ZHANG Q P, ZHANG Y, ZHANG Y C, et al. A sparse denoising-based super-resolution method for scanning radar imaging. Remote Sensing, 2021, 13(14): 2768.

[19] TAN K, LU X Y, YANG J C, et al. A novel Bayesian super-resolution method for radar forward-looking imaging based on Markov random field model. Remote Sensing, 2021, 13(20): 4115.

[20] HUO W B, ZHANG Q P, ZHANG Y, et al. A superfast super-resolution method for radar forward-looking imaging. Sensors, 2021, 21(3): 817.

[21] ZHANG Q P, ZHANG Y, ZHANG Y C, et al. Airborne radar super-resolution imaging based on fast total variation method. Remote Sensing, 2021, 13(4): 549.

[22] WANG Y L, WANG Y Z, GUO Z Y. OAM radar based fast super-resolution imaging. Measurement, 2022, 189: 110600.

[23] YANG T, SHI H Y, GUO J W, et al. Orbital angular momentum based super resolution ISAR imaging for maneuvering targets: modeling and performance analysis. Digital Signal Processing, 2021, 117: 103197.

[24] DU L, LIU H W, BAO Z. Using the amplitude fluctuation property of target HRRP for radar automatic target recognition. Proc. of the International Conference on Radar, 2006. DOI: 10.1109/ICR.2006.343563.

[25] DU L, LIU H W, BAO Z, et al. A two-distribution compounded statistical model for radar HRRP target recognition. IEEE Trans. on Signal Processing, 2006, 54(6): 2226–2238.

[26] HAMNER C A, MAIER M W. Methods to reduce range glint in radars. Proc. of the IEEE Aerospace Conference, 1997, 3: 83–102.

[27] ZHAO F, BI L, MIN T, et al. A new method for detecting the presence of multiple unresolved targets. Acta Electonica Sinica, 2010, 38(10): 2258. (in Chinese)

[28] LILLICRAP T P, HUNT J J, PRITZEL A, et al. Continuous control with deep reinforcement learning. https://arxiv.org/abs/1509.02971.
[29] SCHRO D. Expectation maximization algorithm. Journal of Digital Imaging, 2011, 22(5): 483–491.
[30] KAY S M. Fundamentals of statistical signal processing: estimation theory. Upper Saddle River: Prentice Hall, 1993.
[31] MOSCA E. Angle estimation in amplitude comparison monopulse systems. IEEE Trans. on Aerospace and Electronic Systems, 1969(2): 205–212.

Biographies

CAI Tianyi was born in 1983. He received his Ph.D. degree in science of military logistics and military equipment from Naval Aviation University. He is a senior engineer in Sichuan Institute of Aerospace Electronic Equipment. His research interest is radar signal processing.
E-mail: tsaity@163.com

DAN Bo was born in 1985. He received his Ph.D. degree in information and communication engineering from Naval Aviation University. He is a lecturer in Coastal Defense College of Naval Aviation University. His research interests are artificial intelligence and machine learning.
E-mail: lovelin19841204@163.com

HUANG Weibo was born in 1972. He received his Master's degree in business administration from University of South Australia. He is a senior engineer in Sichuan Institute of Aerospace Electronic Equipment. His research interests are radar system design and signal processing.
E-mail: wuhuangac @163.com